'Cycle to cycle' Optimizing Control of Simulated Moving Beds

Cristian Grossmann, Gültekin Erdem, and Manfred Morari
Automatic Control Laboratory, ETH Zurich, Physikstrasse 3, 8092 Zurich, Switzerland

Mohammad Amanullah and Marco Mazzotti
Institute of Process Engineering, ETH Zurich, Sonneggstrasse 3, 8092 Zurich, Switzerland

Massimo Morbidelli
Institute for Chemical and Bio-Engineering, ETH Zurich, 8092 Zurich, Switzerland

DOI 10.1002/aic.11346
Published online December 3, 2007 in Wiley InterScience (www.interscience.wiley.com).

The novel feature of the presented simulated moving bed (SMB) controller is its capability to make use of the average outlet concentration of the product streams over a cycle as feedback information, i.e., 'cycle to cycle' control. Its effectiveness is confirmed experimentally on an eight-column four-section laboratory SMB unit, which is used to separate a binary mixture of the nucleosides, uridine and guanosine. The performance of the 'cycle to cycle' SMB control scheme is also demonstrated by several SMB simulation runs that are chosen to test the robustness of the controller. Furthermore, the case where measurements have a time delay is presented. The results illustrate that the 'cycle to cycle' controller is able to meet the products' purity specifications and operate the process optimally with minimal information about the system regardless of the disturbances that might take place during the operation. © 2007 American Institute of Chemical Engineers *AIChE J,* 54: 194–208, 2008

Keywords: simulated moving bed, repetitive model predictive control, nucleoside separation, online monitoring, dynamic optimization

Introduction

Simulated moving bed (SMB) is a continuous chromatographic process to separate mixtures into two fractions. The separation principle is the different affinity of the components in the mixture to the solid phase, which moves countercurrently to the direction of the fluid. The generation of a real countercurrent flow between a solid and a fluid phase is impractical to implement and operate, but it can be overcome by a technical approximation of the process, the SMB. The SMB consists of a loop of n_{col} fixed-bed columns where the fluid circulates in one direction (Figure 1). The desired countercurrent flow is achieved by periodically switching the inlet and outlet streams in the direction of the fluid flow, which results in a "simulated" countercurrent movement of the solid with respect to the fluid. A detailed description of the process can be found elsewhere.[1]

There are two main advantages of the SMB process. First, compared to batch chromatography it has a high productivity and low-solvent consumption, which results in lower production costs. Secondly, SMB allows for a fast and reliable scale up of separations from analytical chromatography to production scale, and, therefore, a shorter time to market.

These economical advantages have firmly established SMB in recent years as the state of the art technology for complex separation tasks in the areas of pharmaceuticals,

Correspondence concerning this article should be addressed to M. Morari at morari@control.ee.ethz.ch.

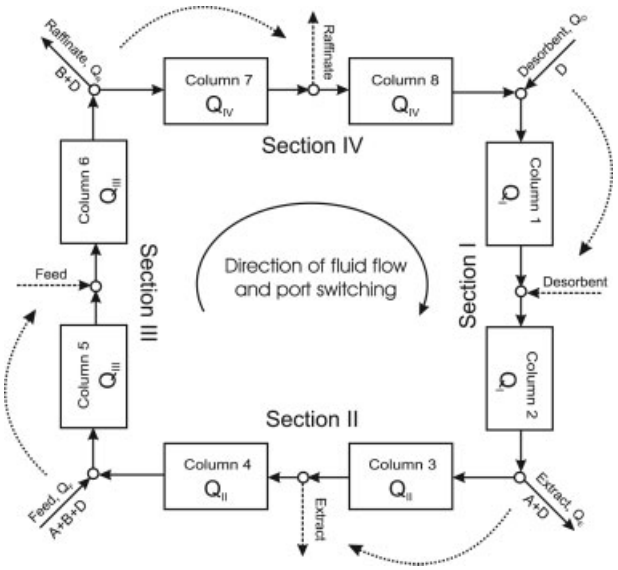

Figure 1. Scheme of the SMB unit considered in this work.

The dashed lines indicate the inlet/outlet positions after the first switch.

fine chemicals and biotechnology. Currently, SMB is rapidly gaining attention for the purification of species characterized by low selectivities, such as chiral molecules for single enantiomer drug development.[2]

However, the robust and optimal operation of the SMB process is still an open problem in practice. The full economical potential of the SMB can be exploited by using a proper feedback control scheme. Several approaches have been proposed.[3–16] A detailed review of these different control schemes may be found in the literature.[17,18] In general, the drawback of these approaches is the need for accurate data about the system.

In the past years the control group at ETH Zurich proposed and verified experimentally an SMB control scheme, which guarantees the fulfillment of product and process specifications, such as minimum purities and maximum allowable pressure drop, while optimizing the economics of the process.[17–23] It is noteworthy that this controller requires only minimal information on both, the adsorption behavior of the components to separate, i.e., only the linear adsorption isotherm, and the characteristics of the columns constituting the SMB unit, i.e., only the average void fraction of the columns in the SMB loop. In this control scheme the concentration levels of both species at the extract and raffinate streams are monitored with online optical detectors, i.e., detectors measuring the absorbance of light or the rotation of polarized light, such as UV or polarimeter detectors, respectively. The choice of these instruments will depend on the nature of the mixture to be separated. This information is fed back to the controller with a relatively high-frequency, i.e., every five seconds, in order to take the appropriate control actions.

The high-sensitivity of the accuracy of the optical detectors to experimental factors, like impurities in the system or pressure fluctuation in the measuring cell, has a direct impact on the performance of the controller.

This article presents a new control scheme, i.e., the 'cycle to cycle' control, that overcomes the limitations imposed by the optical detectors and provides the flexibility to apply the controller to a wider range of separation tasks. This comes from the fact that the 'cycle to cycle' control scheme uses less frequent feedback information obtained by more accurate analytical methods that can be applied to a broader range of mixtures. Furthermore, these kind of measurements are already available in industrial SMB applications, since it is a common practice to collect samples of the outlet streams over a cycle and determine its composition using an automated HPLC system to monitor the quality of the product.

This approach has, on one hand, the advantage that the HPLC measurements are straightforward, more accurate than online optical detectors, can handle multicomponent systems and are not greatly affected by impurities. On the other hand, these measurements are less frequent and provide only information about the *average* concentration of the two species at the outlet streams. Moreover, the analysis time may be in order of the cycle time, which would introduce a significant time delay in the measurements. Hence, the controller relies on less, but more accurate and easy-to-access information that is available with a lower frequency, i.e., once every cycle, and can be delayed.

The effectiveness of this control approach is assessed and demonstrated through experiments on a laboratory SMB unit for the separation of a mixture of nucleosides namely uridine and guanosine, characterized by linear isotherms. Besides, extensive simulations for the same system under various scenarios are performed to challenge the performance of the controller and its robustness to the most relevant disturbances.

This article is structured as follows: the SMB Unit section gives a brief description of the SMB process considered in this work. The 'Cycle to Cycle' Control Concept section explains in detail the development of the controller. The Experimental implementation section presents the results obtained from the validation of the control scheme on a lab-scale SMB plant for the separation of uridine and guanosine under linear chromatographic conditions. Then simulation results for the same system with an additional time delay in the measurements are discussed. Finally, conclusions are presented.

SMB Unit

The SMB unit considered in this work has been presented and extensively described in our previous works.[18] For the sake of completeness, a short summary is given here. A detailed description of the SMB process and its working principle may be found elsewhere.[1]

The mixture of guanosine (A) and uridine (B) is to be separated in a closed-loop four-section eight-column SMB unit arranged in a 2-2-2-2 configuration (see Figure 1). Each column has a volume V and a porosity ε. The dynamical model of the SMB unit is obtained by interconnecting the dynamical models of each chromatographic column. The single-column dynamics are modeled with the equilibrium dispersive model (EDM), and the adsorption behavior of both components inside the columns is described by a linear adsorption isotherm. The mathematical model is completed by consider-

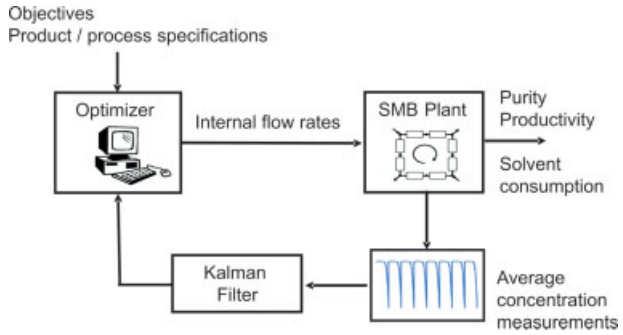

Figure 2. 'Cycle to cycle' control concept.

[Color figure can be viewed in the online issue, which is available at www.interscience.wiley.com.]

ing the corresponding node balances between the columns and the proper boundary and initial conditions.

The physical parameters of the laboratory and virtual SMB plants are given in the Experimental implementation section.

'Cycle to Cycle' Control Concept

For the control concept presented in this work we follow the same philosophy adopted in our previous studies,[21] to integrate the optimization and control of the SMB unit. The novel feature in this concept is that the formulation of the control problem allows to perform measurements, optimization and take control actions only once every cycle, i.e., on a 'cycle to cycle' basis. The control concept is shown in Figure 2.

The control problem is formulated as a constrained dynamic optimization problem within the repetitive model predictive control (RMPC) framework. The productivity and solvent consumption represent the cost function to be optimized, while the hardware restrictions and product quality specifications are imposed as constraints. The controller makes use of a simplified 'cycle to cycle' SMB model to predict and optimize the performance of the unit over a predefined number of cycles, the so-called prediction horizon n_p. The simplified 'cycle to cycle' SMB model requires only the linear isotherm information and the average bed porosity. The solution of the optimization problem yields a sequence of optimal control actions for a chosen number of cycles, namely the control horizon n_c. This scheme is implemented according to a receding horizon strategy, i.e., the optimal control input corresponding to the current cycle is implemented, and the remaining calculated optimal inputs are discarded. The prediction horizon is shifted by one cycle and an optimization problem based on the new estimate of the plant state is solved. The new state estimate is calculated using a filter,[27] and the measurements as they become available.

In this approach the switch time t^* is fixed *a priori*. The internal flow rates in the four sections of the unit Q_I, Q_{II}, Q_{III}, Q_{IV}, are used as manipulated variables. The measured variables are the concentration levels in the extract (E) and raffinate (R) streams averaged over one cycle $c^E_{A,ave}$, $c^E_{B,ave}$, $c^R_{A,ave}$, $c^R_{B,ave}$.

The Simplified 'cycle to cycle' SMB model section is devoted to illustrate the development of the simplified 'cycle to cycle' SMB model used for control purposes. The Repetitive model predictive control formulation to Optimization of the performance sections present how this model is formulated within the RMPC framework, extended to account for time delays in the measurements and built into the scheme in Figure 2.

Simplified 'cycle to cycle' SMB model

A flow chart summarizing the steps involved in the development of the controller is given in Figure 3. To start, the system of partial differential equations (PDEs), resulting from the EDM is discretized in space and linearized.

Making use of the only available information about the mixture to be separated, i.e., the Henry constants H_A and H_B and the average bed porosity ε_{ave}, the linearization point is chosen with help of the triangle theory to fulfill the following conditions[1]

$$0 < m_I^{ref} < H_A \tag{1}$$

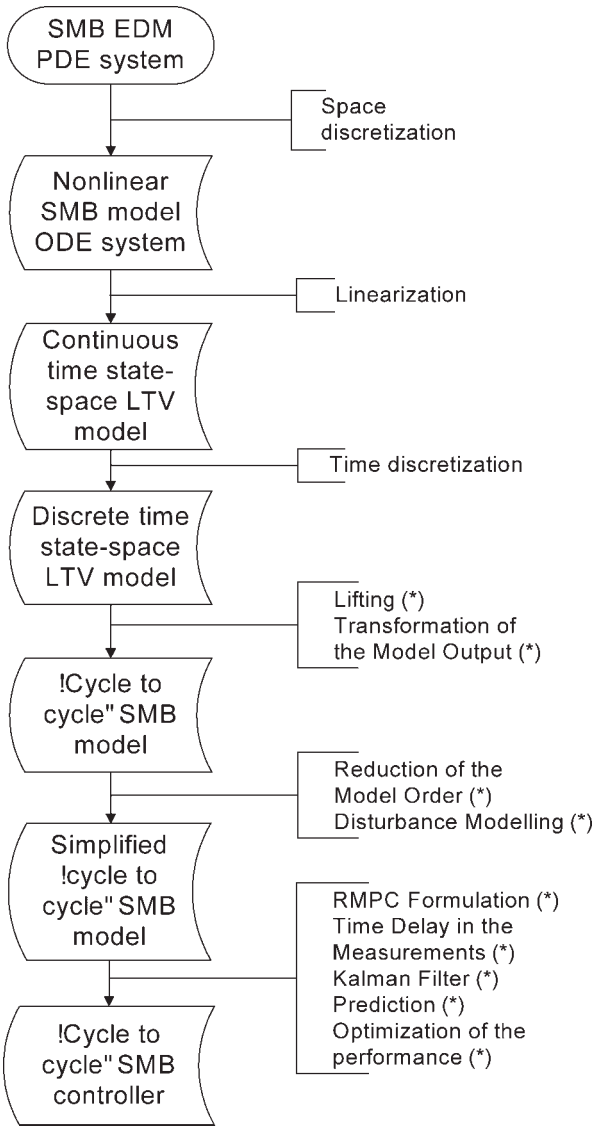

Figure 3. Flow chart summarizing the steps in the development of the 'cycle to cycle' controller.

The steps denoted with (*) will be presented in detail.

$$0 < m_{II}^{ref} < H_B \tag{2}$$

$$H_A < m_{III}^{ref} < \infty \tag{3}$$

$$H_B < m_{IV}^{ref} < \infty \tag{4}$$

where m_j^{ref} are the flow rate ratios for sections $j = I, \ldots, IV$

$$m_j^{ref} = \frac{Q_j^{ref} t^* - V\varepsilon_{ave}}{V(1-\varepsilon_{ave})} \tag{5}$$

It is important to chose the m_j^{ref} values in the conditions 1–4 to lie close to their boundaries with respect to the Henry constants, though fulfilling the inequalities strictly. In our case a margin of ca. 5% of the respective Henry constant was chosen. The reference internal flow rates Q_j^{ref} can be computed from the conditions 1–4 once the switch time t^* has been fixed. Note that according to the triangle theory, these conditions will cause incomplete separation of the species in both outlet streams, as well as regeneration problems in the solid and liquid phase. Nevertheless, this is a good choice for the linearization point because the effect of the manipulated variables will be clearly seen in all measured variables. In contrast, choosing a linearization point that guarantees complete separation of the species and no regeneration problems, would give a poor linear model since some of the input-output sensitivities become zero under these conditions.

The linearized model is subsequently discretized in time, details can be found elsewhere.[21] The resulting discrete time, state-space, linear time-varying (LTV) SMB model has the following structure

$$\begin{aligned} x_k(n+1) &= A(n)x_k(n) + B(n)u_k(n) \quad x \in \mathbf{R}^{n_{eq}},\ u \in \mathbf{R}^{n_u},\ y \in \mathbf{R}^{n_y} \\ y_k(n) &= C(n)x_k(n) \qquad \text{for} \quad n = 0, \ldots, N-1 \end{aligned} \tag{6}$$

Here, k is the cycle index, and n is the time index running within the cycle index; N is the number of time steps within a cycle used for time discretization. The variables x and u are the state and input vectors comprising the internal concentration profiles and the internal flow rates, respectively. The concentration levels of both species A and B, at the two outlet streams, i.e., $[c_A^E(n), c_B^E(n), c_A^R(n), c_B^R(n)]$, constitute the output vector y. The parameters n_{eq}, n_y and n_u indicate the dimension of the state x, and the number of process inputs u and outputs y, respectively. The state, input and output vectors are defined in terms of deviation variables with respect to the reference values.

For the transition from one cycle to the next, we impose the continuity requirement

$$x_{k+1}(0) = x_k(N) \tag{7}$$

The output $y_k(n)$ of the LTV model in Eq. 6 describes the instantaneous concentrations of both components in the two outlets streams for each time step n within the cycle k. In the 'cycle to cycle' control concept the measured variables are the concentration of both species in extract and raffinate *averaged over one cycle*. Therefore, the LTV model has to be modified, such that the required average concentrations are directly given by the model output, i.e., a 'cycle to cycle' SMB model. This procedure is described in the following two subsections.

Lifting the LTV Model. The first step towards a 'cycle to cycle' SMB model is to relate the initial states of two consecutive cycles $x_k(0)$ and $x_{k+1}(0)$. Note that the LTV model in Eq. 6 relates two time steps within the same cycle, i.e., $x_k(n)$ and $x_k(n+1)$. By successive substitution of Eq. 6 for N time steps, i.e., by lifting the LTV model, the desired relationship is obtained. The time-invariant 'cycle to cycle' SMB model can be written as

$$\begin{aligned} x_{k+1}(0) &= \mathbf{\Phi}x_k(0) + \mathbf{\Gamma}\mathbf{U}_k \quad x \in \mathbf{R}^{n_{eq}},\ \mathbf{U} \in \mathbf{R}^{(N\times n_u)} \\ \mathbf{Y}_k &= \mathbf{\Pi}x_k(0) + \mathbf{G}\mathbf{U}_k \quad \mathbf{Y} \in R^{(N\times n_y)} \end{aligned} \tag{8}$$

where Φ, Γ, Π and $\mathbf{G}$ are

$$\mathbf{\Phi} = A(N-1)A(N-2)\cdots A(0) \tag{9}$$

$$\mathbf{\Gamma} = \left[\left(A(N-1)\cdots A(1)B(0)\right)\left(A(N-1)\cdots A(2)B(1)\right)\ \cdots\ B(N-1)\right] \tag{10}$$

$$\mathbf{\Pi} = \begin{bmatrix} C(0) \\ C(1)A(0) \\ \vdots \\ C(N-1)A(N-2)\cdots A(0) \end{bmatrix} \tag{11}$$

$$\mathbf{G} = \begin{bmatrix} 0 & 0 & \cdots & 0 & 0 \\ C(1)B(0) & 0 & \cdots & 0 & 0 \\ C(2)A(1)B(0) & C(2)B(1) & \cdots & 0 & 0 \\ \vdots & \vdots & \vdots & \vdots & \vdots \\ (C(N-1)A(N-2)\cdots A(1)B(0)) & \cdots & \cdots & C(N-1)B(N-2) & 0 \end{bmatrix} \tag{12}$$

The inputs and outputs of one cycle are grouped in $\mathbf{Y}_k$ and $\mathbf{U}_k$

$$\mathbf{Y}_k = \left[y_k^T(0)\ \cdots\ y_k^T(N-1)\right]^T \tag{13}$$

$$\mathbf{U}_k = \left[u_k^T(0)\ \cdots\ u_k^T(N-1)\right]^T \tag{14}$$

Note that $\mathbf{Y}_k$ contains the concentrations of both species for every time step $n = 0, \ldots, N-1$ of cycle k.

Transformation of the Model Output. The last step to obtain the 'cycle to cycle' SMB model is to compute the average of the time-varying concentrations contained in $\mathbf{Y}_k$

$$y_{k,ave} = \frac{\sum_{n=0}^{N-1} y_k(n)}{N} = \mathcal{C}\mathbf{Y}_k \tag{15}$$

Under the assumption of constant flow rates within one cycle, the desired average concentrations $y_{k,ave}$ are a linear combination of the output vector $\mathbf{Y}_k$. $\mathcal{C}$ is the transformation matrix relating these two vectors. By inserting the model output expression from Eq. 8 into Eq. 15 we get

$$y_{k,ave} = \mathcal{C}(\mathbf{\Pi}x_k(0) + \mathbf{G}\mathbf{U}_k) = \underbrace{\mathcal{C}\mathbf{\Pi}}_{\bar{\mathbf{\Pi}}} x_k(0) + \underbrace{\mathcal{C}\mathbf{G}}_{\bar{\mathbf{G}}} \mathbf{U}_k \tag{16}$$

Finally, the 'cycle to cycle' SMB model providing the average concentrations as output can be cast as

$$\begin{aligned} x_{k+1}(0) &= \mathbf{\Phi}x_k(0) + \mathbf{\Gamma}\mathbf{U}_k \quad x \in \mathbf{R}^{n_{eq}},\ \mathbf{U} \in \mathbf{R}^{(N\times n_u)} \\ y_{k,ave} &= \bar{\mathbf{\Pi}}x_k(0) + \bar{\mathbf{G}}\mathbf{U}_k \quad y_{ave} \in \mathbf{R}^{n_y} \end{aligned} \tag{17}$$

Reduction of the Model Order. For the system considered in this study, i.e., a binary mixture to be separated in an eight-column SMB unit with a number of grid points $n_g = 40$ along each column, the model has 640 states. This may lead to a very big computational load. Fortunately, well established model reduction techniques are available. Here, the balanced model order reduction was used,[28–30] and the number of states in Eq. 17 was reduced from $n_{eq} = 640$ to $\tilde{n}_{eq} = 26$.

Disturbance Modeling. The system is subjected to various types of disturbances which have to be handled by the controller. Therefore, accounting for the combined overall effect of all possible disturbances on the plant output is a critical issue for the control performance. The disturbances affecting SMB units can be divided into two categories. The first one are periodic disturbances with period of one cycle, e.g., changes in the feed concentration during operation due to different feed batches of the mixture to be separated. The second category consists of random disturbances, which do not repeat every cycle.

The effect of unknown model errors and both type of disturbances are incorporated into the outputs of the reduced-order 'cycle to cycle' SMB model as a residual term $\mathbf{h}_k$

$$\tilde{x}_{k+1}(0) = \tilde{\mathbf{\Phi}}\tilde{x}_k(0) + \tilde{\mathbf{\Gamma}}\mathbf{U}_k \quad \tilde{x} \in \mathbf{R}^{\tilde{n}_{eq}},\ \mathbf{U} \in \mathbf{R}^{(N\times n_u)} \tag{18}$$

$$y_{k,ave} = \tilde{\mathbf{\Pi}}\tilde{x}_k(0) + \bar{\mathbf{G}}\mathbf{U}_k + \mathbf{h}_k \quad y_{ave} \in \mathbf{R}^{n_y},\ \mathbf{h} \in \mathbf{R}^{n_y} \tag{19}$$

where $\tilde{\mathrm{x}}$ is the state vector of the reduced-order 'cycle to cycle' SMB model, and $\tilde{\mathbf{\Phi}}$, $\tilde{\mathbf{\Gamma}}$, $\tilde{\mathbf{\Pi}}$ and $\overline{\mathbf{G}}$ are the state-space matrices. The residual term $\mathbf{h}_k$ is modeled with the stochastic difference equation

$$\bar{\mathbf{h}}_{k+1} = \bar{\mathbf{h}}_k + \boldsymbol{w}_k \tag{20}$$

$$\mathbf{h}_k = \bar{\mathbf{h}}_k + \boldsymbol{v}_k \tag{21}$$

Here, $\boldsymbol{w}_k$ represents the effect of model errors and periodic disturbances and is integrated from cycle to cycle in the term $\bar{\mathbf{h}}_k$. The vector $\boldsymbol{v}_k$ can be interpreted as the part that represents the effect of random disturbances. Both $\boldsymbol{w}_k$ and $\boldsymbol{v}_k$ are zero-mean white-noise sequences with respect to the cycle index and covariance matrices R_w and R_v, respectively.

Repetitive model predictive control formulation

So far, a simplified 'cycle to cycle' SMB model that incorporates the effects of model errors and disturbances has been developed. In this section, it is reformulated within the repetitive model predictive control (RMPC) framework.

For the sake of clarity in the index notation, it is important to note that the earliest measurement of the average concentrations for cycle $k-1$, $y_{k-1,ave}$, can be completed at the end of cycle $k-1$, that formally corresponds to the sampling performed at time instance k. This represents an inherent time delay in the system. The same applies to the noise sequences $\boldsymbol{w}_{k-1}$ and $\boldsymbol{v}_{k-1}$ that are sampled at time k. Thus, we define for control purposes

$$\begin{aligned} \bar{\mathbf{y}}_k &\triangleq \tilde{\mathbf{\Pi}}\tilde{x}_{k-1}(0) + \bar{\mathbf{G}}\mathbf{U}_{k-1} + \bar{\mathbf{h}}_{k-1} \\ \bar{\boldsymbol{w}}_k &\triangleq \boldsymbol{w}_{k-1} \\ \bar{\boldsymbol{v}}_k &\triangleq \boldsymbol{v}_{k-1} \end{aligned} \tag{22}$$

the newly defined $\bar{\mathbf{y}}_k$ represents the average concentrations of cycle $k-1$, $y_{k-1,ave}$ according to Eq. 17, plus the integrated effect of model errors and periodic disturbances $\bar{\mathbf{h}}_{k-1}$ from Eq. 20. The effect of random disturbances is incorporated with the term $\bar{\boldsymbol{v}}_k$. Eq. 19 can be written in terms of the new variables to define

$$\mathbf{y}_k \triangleq \bar{\mathbf{y}}_k + \bar{\boldsymbol{v}}_k \tag{23}$$

where $\mathbf{y}_k$ are the model outputs that will be measured at time k. Using these definitions, Eqs. 18 and 19 can be rewritten in terms of incremental changes by differencing the model equations for two successive cycles

$$\underbrace{\begin{bmatrix} \Delta\tilde{x}_{k+1}(0) \\ \bar{\mathbf{y}}_{k+1} \end{bmatrix}}_{z_{k+1}} = \underbrace{\begin{bmatrix} \tilde{\mathbf{\Phi}} & 0 \\ \tilde{\mathbf{\Pi}} & I \end{bmatrix}}_{\bar{A}} \underbrace{\begin{bmatrix} \Delta\tilde{x}_k(0) \\ \bar{\mathbf{y}}_k \end{bmatrix}}_{z_k} + \underbrace{\begin{bmatrix} \tilde{\mathbf{\Gamma}} \\ \bar{\mathbf{G}} \end{bmatrix}}_{\bar{B}} \Delta\mathbf{U}_k + \underbrace{\begin{bmatrix} 0 \\ I \end{bmatrix}}_{\bar{L}} \bar{\boldsymbol{w}}_k \tag{24}$$

$$\mathbf{y}_k = \underbrace{\begin{bmatrix} 0 & I \end{bmatrix}}_{\bar{C}} \underbrace{\begin{bmatrix} \Delta\tilde{x}_k(0) \\ \bar{\mathbf{y}}_k \end{bmatrix}}_{z_k} + \underbrace{[0]}_{\bar{D}} \Delta\mathbf{U}_k + \underbrace{[I]}_{\bar{H}} \bar{\boldsymbol{v}}_k \tag{25}$$

where $\Delta\tilde{\mathrm{x}}_k = (\tilde{\mathrm{x}}_k(0) - \tilde{\mathrm{x}}_{k-1}(0))$, $\Delta\mathbf{U}_k = (\mathbf{U}_k - \mathbf{U}_{k-1})$. In this way, the 'cycle to cycle' SMB model can be cast in the following compact form, which constitutes the basis for the formulation of the control problem

$$\begin{aligned} z_{k+1} &= \bar{A}z_k + \bar{B}\Delta\mathbf{U}_k + \bar{L}\bar{\boldsymbol{w}}_k \quad z \in \mathbf{R}^{\tilde{n}_{eq}+n_y},\ \mathbf{U} \in \mathbf{R}^{N\times n_u} \\ \mathbf{y}_k &= \bar{C}z_k + \bar{D}\Delta\mathbf{U}_k + \bar{H}\bar{\boldsymbol{v}}_k \quad \mathbf{y} \in \mathbf{R}^{n_y} \end{aligned} \tag{26}$$

Time delay in the measurements

A time delay in the measurements is unavoidable whenever these are performed by devices that involve analysis times in the range of minutes, e.g., HPLC. The 'cycle to cycle' SMB model can be extended to account for this fact.

For the sake of generality, it is assumed that the measurements are delayed by n_{td} cycles, i.e., the average concentrations of cycle k are available at time instance $k + 1 + n_{td}$, where the 1 comes from the inherent time delay of the system discussed in the Repetitive model predictive control formulation section. We generalize the definition in Eq. 23 to

$$\mathbf{y}_k \triangleq \bar{\mathbf{y}}_{k-n_{td}} + \bar{\boldsymbol{v}}_{k-n_{td}} \tag{27}$$

Note that $\bar{\mathbf{y}}_{k-n_{td}}$ is contained within the state $z_{k-n_{td}}$, see Eq. 24. Therefore, the state z_k is augmented with the past states $[z_{k-1}^T \ \dots \ z_{k-n_{\text{td}}}^T]^T$ and inputs $[\Delta\mathbf{U}_{k-1}^T \ \dots \ \Delta\mathbf{U}_{k-n_{\text{td}}}^T]^T$

$$Z_k^{(n_{td})} = \left[\underbrace{z_k^T}_{\tilde{n}_{eq}+n_y} \quad \underbrace{z_{k-1}^T \ \dots \ z_{k-n_{td}}^T}_{n_{td}\cdot(\tilde{n}_{eq}+n_y)} \quad \underbrace{\Delta\mathbf{U}_{k-1}^T \ \dots \ \Delta\mathbf{U}_{k-n_{td}}^T}_{n_{td}\cdot(N\cdot n_u)} \right]^T \tag{28}$$

Furthermore we define

$$\begin{aligned} \bar{\bar{\boldsymbol{w}}}_k &\triangleq \boldsymbol{w}_{k-1-n_{td}} \\ \bar{\bar{\boldsymbol{v}}}_k &\triangleq \boldsymbol{v}_{k-1-n_{td}} \end{aligned} \tag{29}$$

Analogous to Eq. 26, the 'cycle to cycle' SMB model for the case of n_{td} cycles of time delay in the measurements can be written as

$$\begin{aligned} Z_{k+1}^{(n_{td})} &= \bar{A}^{(n_{td})} Z_k^{(n_{td})} + \bar{B}^{(n_{td})} \Delta\mathbf{U}_k + \bar{L}^{(n_{td})} \bar{\bar{\boldsymbol{w}}}_k \\ \mathbf{y}_k &= \bar{C}^{(n_{td})} Z_k^{(n_{td})} + \bar{D}^{(n_{td})} \Delta\mathbf{U}_k + \bar{H}^{(n_{td})} \bar{\bar{\boldsymbol{v}}}_k \end{aligned} \tag{30}$$

For $n_{td} = 0$, Eq. 30 corresponds to Eq. 26. For $n_{td} > 0$, a detailed description to build the matrices $\overline{A}^{(n_{td})}$, $\overline{B}^{(n_{td})}$, $\overline{C}^{(n_{td})}$, $\overline{D}^{(n_{td})}$, $\overline{L}^{(n_{td})}$ and $\overline{H}^{(n_{td})}$ is provided in the Appendix.

Kalman filter

A linear time-invariant Kalman filter is used for linear optimal state estimation.[27] The state estimate of cycle $k - 1$, $\hat{\mathrm{z}}(k - 1|k - 1)$, is used to predict the state estimate of cycle k

$$\hat{z}(k|k-1) = \bar{A}\hat{z}(k-1|k-1) + \bar{B}\Delta\mathbf{U}_{k-1} \tag{31}$$

$$\hat{\mathbf{y}}(k|k-1) = \bar{C}\hat{z}(k|k-1) \tag{32}$$

where $\hat{\mathrm{z}}(k|k - 1)$ and $\hat{\mathrm{y}}(k|k - 1)$ denote the estimate of z_k and $\mathbf{y}_k$, respectively, based on information available up to time $k - 1$. In the case of time delay in the measurements, the matrices $\overline{A}$, $\overline{B}$ and $\overline{C}$ become $\overline{A}^{(n_{td})}$, $\overline{B}^{(n_{td})}$ and $\overline{C}^{(n_{td})}$. Note that $\overline{D}$ does not appear in Eq. 32 since $\overline{D}^{(n_{td})} = 0$ for $n_{td} \geq 0$. The state estimate $\hat{\mathrm{z}}(k|k - 1)$ can be corrected given the measurements of the plant $\mathbf{y}^{meas}(k)$

$$\hat{z}(k|k) = \hat{z}(k|k-1) + M[\mathbf{y}^{meas}(k) - \hat{\mathbf{y}}(k|k-1)] \tag{33}$$

where M represents the filter gain matrix that is computed from the steady state solution of the Riccati difference equation.[27] Inserting Eq. 31 into Eq. 33 yields

$$\begin{aligned} \hat{z}(k|k) = \bar{A}\hat{z}(k-1|k-1) + \bar{B}\Delta\mathbf{U}_{k-1} \\ + M[\mathbf{y}^{meas}(k) - \hat{\mathbf{y}}(k|k-1)] \end{aligned} \tag{34}$$

Prediction

The 'cycle to cycle' SMB model is used to predict the behavior of the plant for n_p steps ahead, as a function of the state estimate, and n_c future inputs

$$\mathcal{Y}^{n_p}(k + n_p|k) = S^z \hat{z}(k|k) + S^u \Delta\mathcal{U}_k^{n_c} \tag{35}$$

where $\hat{\mathrm{z}}(k|k)$ is the state estimate obtained from the observer Eq. 34. $\mathcal{Y}^{n_p}(k + n_p|k)$ and $\Delta\mathcal{U}_k^{n_c}$ concatenate the output predictions from $k + 1$ to $k + n_p$ based on the information up to time k, and the control inputs for the next n_c time steps, respectively. The latter one represents the optimization variable

$$\mathcal{Y}^{n_p}(k + n_p|k) = \begin{bmatrix} \hat{\mathbf{y}}(k+1|k) \\ \vdots \\ \hat{\mathbf{y}}(k+n_p|k) \end{bmatrix} \quad \Delta\mathcal{U}_k^{n_c} = \begin{bmatrix} \Delta\mathbf{U}_k \\ \vdots \\ \Delta\mathbf{U}_{k+n_c-1} \end{bmatrix} \tag{36}$$

The prediction matrices S^z and S^u are built by successive substitution of Eqs. 31 and 32.

Optimization of the performance

The controller has two main tasks. First, it should fulfill the product specifications while respecting the process constraints. Second, the controller should optimize the performance of the unit with respect to a given economic criterion. These tasks can be cast as a linear program (LP), which will be described in this section. The main idea is to incorporate the product specifications and process limitations as constraints in the LP, while the economic criteria represent the objective function for the optimization problem.

The product is required to have a minimum purity. Keeping the flow rates of the four sections constant within the cycle, the average purities are defined as

$$P_{k,ave}^E = \frac{c_{A,k,ave}^E}{c_{A,k,ave}^E + c_{B,k,ave}^E} \tag{37}$$

$$P_{k,ave}^R = \frac{c_{B,k,ave}^R}{c_{A,k,ave}^R + c_{B,k,ave}^R} \tag{38}$$

Equations 37 and 38 are nonlinear functions of the concentration terms, and have to be linearized to be compatible with the LP formulation. The estimated outlet concentrations of cycle k are used as linearization points for cycle $k + 1$, and can be updated every cycle according to the state estimate. The constraints for minimum purity over the prediction horizon n_p, can then be formulated as

$$P_{l,ave}^E \geq P_{min}^E - s_1 \quad \text{with} \quad s_1 \geq 0 \tag{39}$$

$$P^R_{l,ave} \geq P^R_{min} - s_2 \quad \text{with} \quad s_2 \geq 0 \quad \text{for} \quad l = k+1, \ldots, k+n_p \quad (40)$$

where s_1 and s_2 are slack variables to avoid infeasibility problems. Note that $P^E_{l,ave}$ and $P^R_{l,ave}$ for $l = k + 1, \ldots, k + n_p$ are computed from the estimation of the future output average concentration values $\hat{c}_{l,ave} = [\hat{c}^E_{A,l,ave}, \hat{c}^E_{B,l,ave}, \hat{c}^R_{A,l,ave}, \hat{c}^R_{B,l,ave}]^T$. Here, $\hat{c}_{l,ave}$ is directly obtained from the output predictions $\mathcal{Y}^{n_p}(k + n_p|k)$ given in Eq. 36.

The input flowrates $\mathbf{Q}_k = [Q_{k,I}, Q_{k,II}, Q_{k,III}, Q_{k,IV}]^T$ and the estimates of the future output average concentration values $\hat{c}_{k,ave}$ must be nonnegative. Slack variables are added to soften the constraints on the outputs

$$\hat{\mathbf{c}}_{l,ave} \geq \mathbf{0} - \mathbf{s}_3 \quad \text{with} \quad \mathbf{s}_3 \geq \mathbf{0} \quad \text{for} \quad l = k+1, \ldots, k+n_p \quad (41)$$

$$\mathbf{Q}_i \geq \mathbf{0} \quad \text{for} \quad i = k, ..., k+n_c-1 \quad (42)$$

The maximum allowable pressure drop consideration and a smooth operation of the plant in terms of maximum allowable changes in the flow rates are formulated as inequality constraints of the following form

$$\mathbf{Q}^{max} \geq \mathbf{Q}_i \quad (43)$$

$$\Delta\mathbf{Q}^{max} \geq |\Delta\mathbf{Q}_i| \quad \text{for} \quad i = k, \ldots, k+n_c-1 \quad (44)$$

where $\Delta\mathbf{Q}_i = \mathbf{Q}_i - \mathbf{Q}_{i-1}$.

It is also advantageous to constrain the changes of each manipulated variable with positive slack variables that are penalized in the cost function with certain weights. On the one hand, this is a way to tune how "expensive" it is for the controller to undertake changes in the manipulated variables, i.e., how fast it should perform the changes on the flow rates. On the other hand, these weights allow expressing a possible preference for the use of one manipulated variable over another

$$|\Delta\mathbf{Q}_i| \leq \mathbf{s}_4 \quad \text{for} \quad i = k, \ldots, k+n_c-1 \quad (45)$$

For the 'cycle to cycle' control, the same flow rates are imposed within a cycle

$$\mathbf{Q}_i(0) = \mathbf{Q}_i(n) \quad \text{for} \quad i = k, \ldots, k+n_c-1 \quad \text{and} \quad n = 1, \ldots, N-1 \quad (46)$$

Finally, the cost function is defined to maximize the feed flow rate Q_F, and minimize the desorbent consumption Q_D over a given control horizon n_c

$$\min_{\Delta\mathcal{U}^{n_c}_k, \mathbf{s}} \left[\sum_{i=k}^{k+n_c-1} \left[\lambda_{i,D} \underbrace{Q_{i,D}}_{Q_{i,I}-Q_{i,IV}} - \lambda_{i,F} \underbrace{Q_{i,F}}_{Q_{i,III}-Q_{i,II}} \right] + \lambda_s \mathbf{s} \right] \quad (47)$$

where λ_D, λ_F and λ_s are the weights assigned to each term in the cost function. The weights λ_D and λ_F reflect the importance given to the desorbent consumption minimization and the feed throughput maximization, respectively; $\mathbf{s}$ is a vector containing the nonnegative slack variables used to soften the constraints.

The sets of inequality (Eqs. 39–45) and equality (Eq. 46) constraints complete the formulation of the LP. For our example system the problem comprises 300 variables, and approximately 400 constraints. A commercial solver, ILOG CPLEX 7.0 was used to solve the optimization problem. The maximum computation time was found to be less than 0.1 s in a PC with a 3 GHz processor.

Experimental Implementation

This section is devoted to the implementation of the control concept on a laboratory SMB plant. The first goal is to experimentally evaluate and demonstrate the capability of the controller to deliver the products with the required specifications, while exploiting the full potential of the SMB process in terms of productivity and solvent consumption. The second goal is to asses the controller performance under uncertainties and disturbances.

The results of the following case studies will be analyzed using the so called triangle theory, a rather standard method for interpreting SMB results.[1] The triangle theory combines the five operating parameters of the SMB, i.e., the four sectional flow rates and the switch time, into four dimensionless numbers, the flow rate ratios, that characterize the performance of the unit

$$m_j = \frac{Q_j t^* - V\varepsilon}{V(1-\varepsilon)} \qquad (j = I, \ldots, IV) \quad (48)$$

Note that the flow rate ratios m_j are linear functions of the flow rates Q_j, when the switch time t^* is fixed.

A summary of the SMB plant parameters and of the properties of the mixture to be separated is given in Table 1, the controller parameters are given in Table 2. A more detailed characterization of the system can be found in one of our earlier studies.[20] A linear adsorption isotherm describes the adsorption behavior accurately in the range of feed concentrations investigated in this work. The outlet concentrations of both species were averaged over one cycle and used for control purposes. Since an online monitoring system using

Table 1. Physical parameters of the SMB laboratory plant and the nucleoside mixture

Parameter	Value
Mixture to be separated	Guanosine (A) and Uridine (B)
Mobile phase	5% ethanol in water
Stationary phase	Source 30 RPC
Feed concentration, [g/L]	0.05 each
Temperature, [$^\circ C$]	23
Number of columns	8
Column distribution	2/2/2/2 Closed loop
Column diameter, [cm]	1
Column length, [cm]	10
Nominal porosity, ε	0.375
Switching time, t^*, [s]	120
Theoretical plates per column	100
Henry constants	$H_A = 2.14$, $H_B = 1.32$

Table 2. The parameters used for the controller synthesis

Parameter	Value	Parameter	Value
N	64	R_w	1000
n_g	40	λ_D	4
$m_{j=I\ldots IV}^{ref}$	2.28, 1.25, 2.29, 1.29	λ_F	20
n_p	8 cycles	λ_s	100
n_c	1 cycle	$P_{\min}^{E}$	99.0%
R_v	1	$P_{\min}^{R}$	99.0%
Henry constants	$H_A = 2.25$, $H_B = 1.30$		

ultraviolet detectors (UV) was already available, we made use of it to get the average concentration information, instead of using HPLC. This also implies for the system studied in the following, that only the inherent cycle of delay in the measurements introduced by the control problem formulation we adopted, will be present. Please refer to the Repetitive model predictive control formulation section for a detailed discussion. The details about the online monitoring system may be found in earlier publications.[17,20]

Case study 1: Plant-model mismatch

The controller is developed using information from pulse injection under dilute condition i.e., only the Henry coefficients, and average porosity of the columns. However, it is common to have uncertainties and errors in these measurements. Besides, temperature deviations, plant dead volumes and aging of the solid phase affect the retention behavior of the species. This may lead to a difference between the actual Henry constants characterizing the plant and the ones provided to the model. In order to demonstrate the controller performance under such conditions, the model is developed based on $H_A^{model} = 2.25$ and $H_B^{model} = 1.30$, which are different from the Henry constants characterizing the plant, namely $H_A^{plant} = 2.14$ and $H_B^{plant} = 1.32$, i.e., 5% smaller and 1% larger, respectively. This specific example might arise from the combination of two rather typical situations in SMB practice, namely temperature deviations and measurement errors, but is aimed at demonstrating the robustness of the controller under a plant-model mismatch.

The first experiment comprises two parts. The first part, i.e., up to cycle 70, addresses the startup of the plant under the plant-model mismatch situation. Figure 4 shows the evolution of extract and raffinate purities and of the cost. The plant was started up with the reference flow rates ($m_I^{ref} = 2.28$, $m_{II}^{ref} = 1.25$, $m_{III}^{ref} = 2.29$, $m_{IV}^{ref} = 1.29$) and clean columns. The controller was switched on at cycle 1. The specified minimum purities were 99.0% for both product streams. The startup point falls within the region, where none of the product streams is pure, see Figure 5. The controller's first priority is to fulfill the product purities, regardless of the operating cost. The actions taken in the first 10 cycles increase the cost function until the specified raffinate and extract product purities are achieved. Once the purity specifications are fulfilled the action of the controller takes the operating point near the vertex of the triangle of the complete separation regime as seen in Figure 5. This clearly demonstrates the capability of the controller to fulfill the required purities, and to optimize the operation under a plant-model mismatch scenario.

Case study 2: Feed pump malfunctioning

This experiment addresses one of the common disturbances in an SMB plant, the malfunctioning of a pump. The

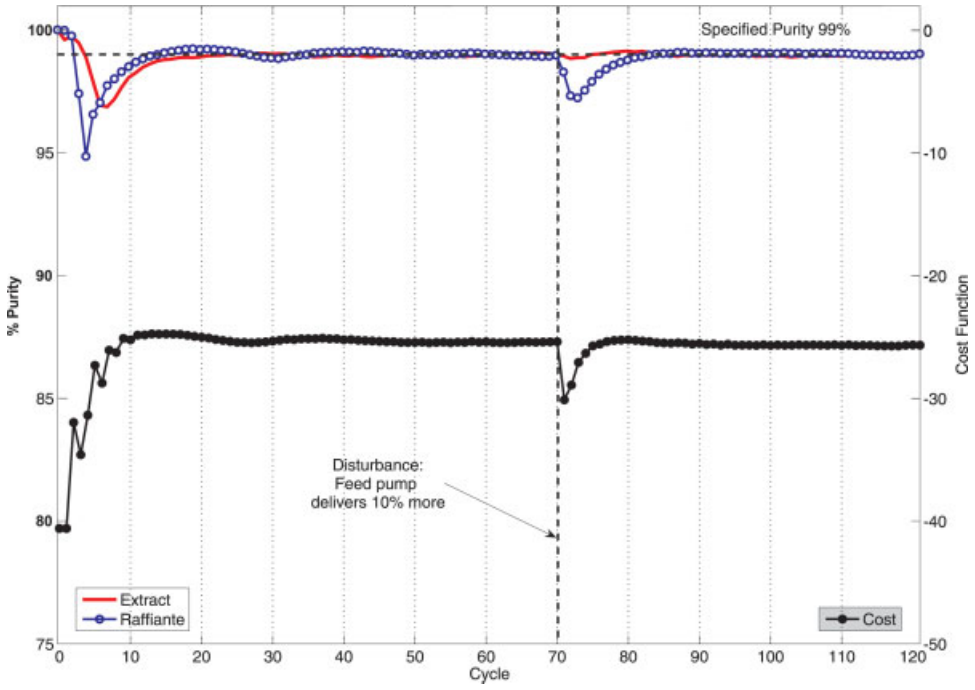

Figure 4. Performance of the controller on the laboratory SMB plant for case studies 1 and 2.

Outlet purities and cost function vs. time measured in cycles. Feed pump delivers 10% more than its set point after cycle 70. [Color figure can be viewed in the online issue, which is available at www.interscience.wiley.com.]

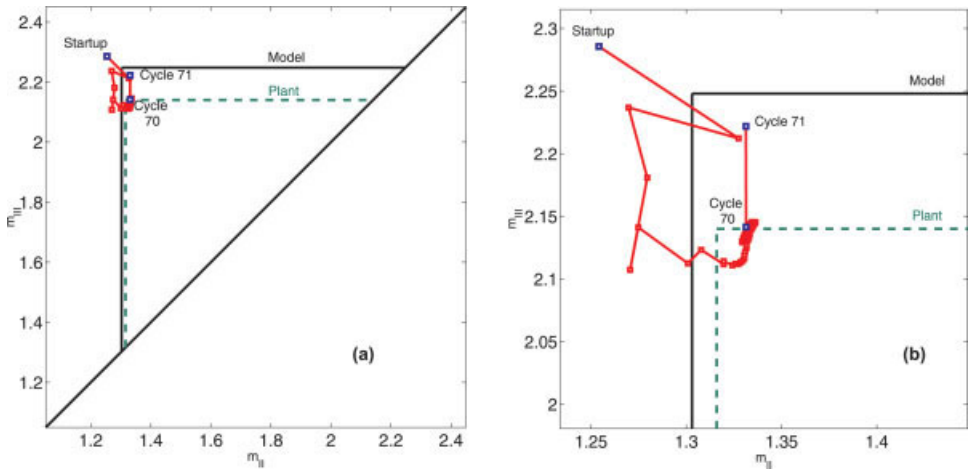

Figure 5. Inputs to the laboratory SMB plant represented in the $m_{II} - m_{III}$ plane for case study 1.

(a) Trajectory of the operation from the startup to cycle 71. (b) Close up. The operating point is taken by the controller from the startup point to the vertex of the complete separation region and remains there until cycle 70. The operating point after the feed pump malfunctioning (discussed in case study 2) is labeled as cycle 71. [Color figure can be viewed in the online issue, which is available at www.interscience.wiley.com.]

results are shown in the second part of Figure 4. between cycle 70 and 120. The steady-state operation at cycle 70 was disturbed by increasing the feed flow rate by 10%. Note that this change is unknown to the controller, and the controller only notices the disturbance by its effect on the measurements. The disturbance increases the flow rates in sections II and III, which can be represented in the $m_{II} - m_{III}$ plane as a shift of the operating point upwards, as depicted in Figure 5 for the operating point at cycle 71. This point lies in the pure extract region, which makes the purity of the raffinate go down. Figure 6 shows the operating trajectory after the disturbance, and how the controller brings back the operating point to the vertex of the complete separation region in order to fulfill again the minimum specified purities and optimize the performance.

Case study 3: Recycle pump malfunctioning

A more challenging scenario of pump malfunctioning is presented in this case study. The recycle pump malfunctioning is a more severe disturbance for the controller to reject, since such a disturbance affects the flow rates in all four sections of the SMB plant. This experiment can be divided into two parts. Cycle 1 to 55 corresponds to the startup of the plant under a plant-model mismatch as discussed in case study 1. The second part starts at cycle 56, when a 5% increase in the recycle pump flow rate was artificially introduced. This again was unknown to the controller.

Figure 7 shows the evolution of the outlet purities and cost function. The plant was started at the reference flow rates, i.e., $m_I^{ref} = 2.28$, $m_{II}^{ref} = 1.25$, $m_{III}^{ref} = 2.29$ and $m_{IV}^{ref} = 1.29$. The columns were clean initially and the controller was switched on at cycle 1. The minimum required purities were 99.0% from both product streams.

As depicted in Figure 8, the disturbance can be represented as a shift up to the right of the operating point at cycle 55 in the $m_{II} - m_{III}$ plane. This is due to an increase of flow in section I, which is directly determined by the recycle pump and makes the flow rates in sections II, III and IV increase as well. The operating point at cycle 56, after the disturbance, lies in the pure extract region in the $m_{II} - m_{III}$ plane, making the purity of extract and raffinate increase and decrease, respectively. The trajectory after the disturbance is depicted in Figure 9.

It is interesting to observe how the controller, in order to improve the low raffinate purity as fast as possible, first

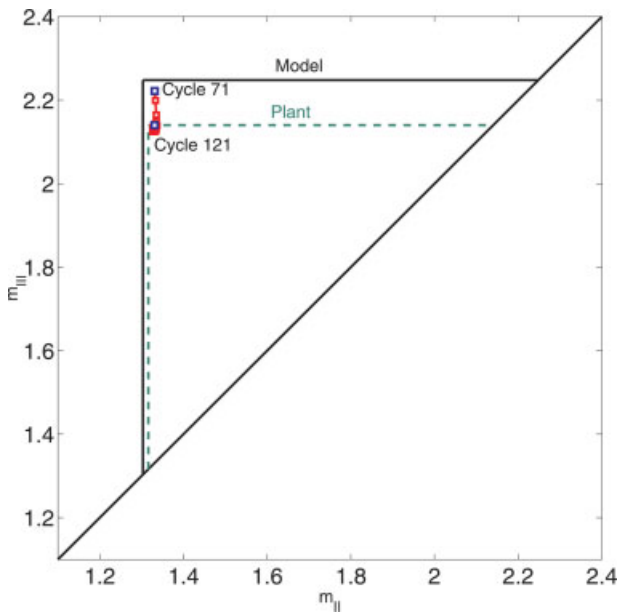

Figure 6. Inputs to the laboratory SMB plant represented in the $m_{II} - m_{III}$ plane for case study 2.

The operating point after the feed pump malfunctioning is labeled as cycle 71. The laboratory SMB plant is brought back by the controller to the vertex of the complete separation region within 15 cycles, and remains there until the end of the operation at cycle 121. [Color figure can be viewed in the online issue, which is available at www.interscience.wiley.com.]

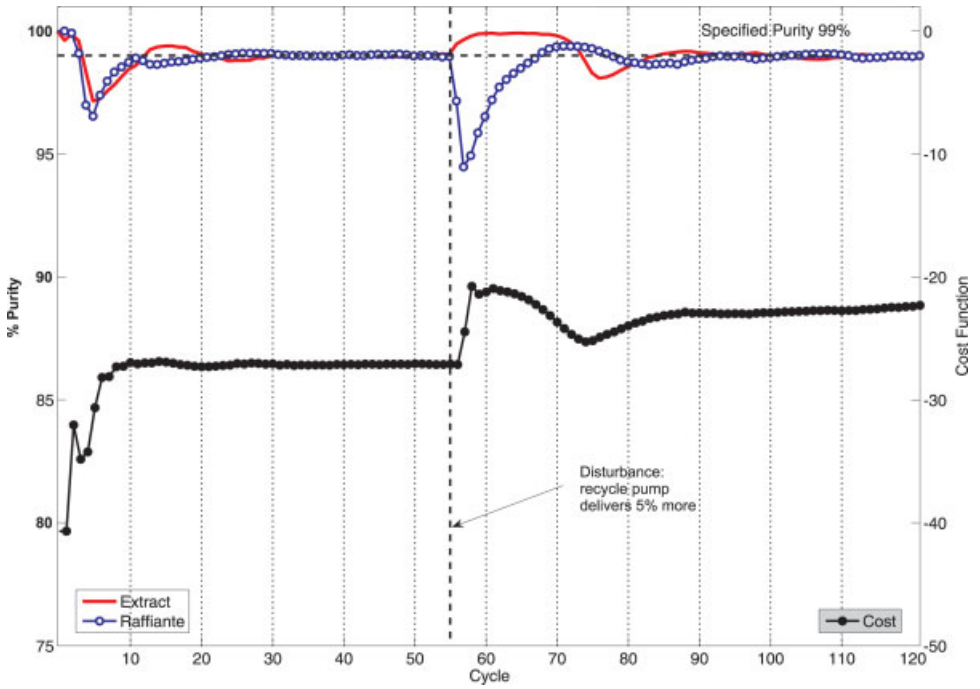

Figure 7. Performance of the controller on the laboratory SMB plant for case study 3.

Outlet purities and cost function vs time measured in cycles. Recycle pump starts to deliver 5% more than its set point at cycle 56. [Color figure can be viewed in the online issue, which is available at www.interscience.wiley.com.]

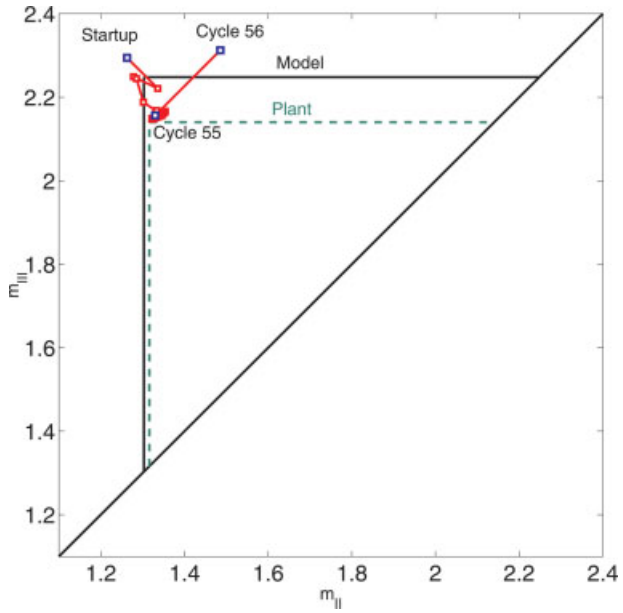

Figure 8. Inputs to the laboratory SMB plant represented in the $m_{II} - m_{III}$ plane for case study 3 from startup up to the malfunctioning of the recycle pump.

The steady state operating point reached after startup is labeled as cycle 55. It is shifted by the recycle pump malfunctioning to the operating point labeled as cycle 56. [Color figure can be viewed in the online issue, which is available at www.interscience.wiley.com.]

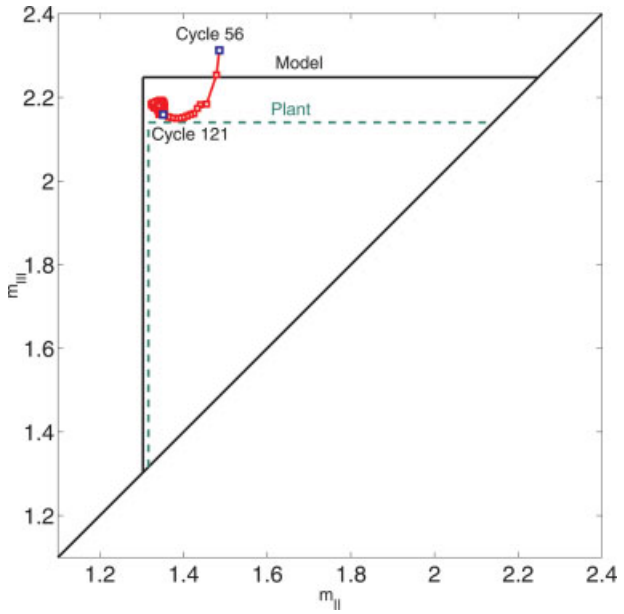

Figure 9. Controller inputs to the laboratory SMB plant represented in the $m_{II} - m_{III}$ plane for case study 3 after the recycle pump malfunctioning.

The disturbed operating point at cycle 56 is brought back to the vertex of the complete separation region. [Color figure can be viewed in the online issue, which is available at www.interscience.wiley.com.]

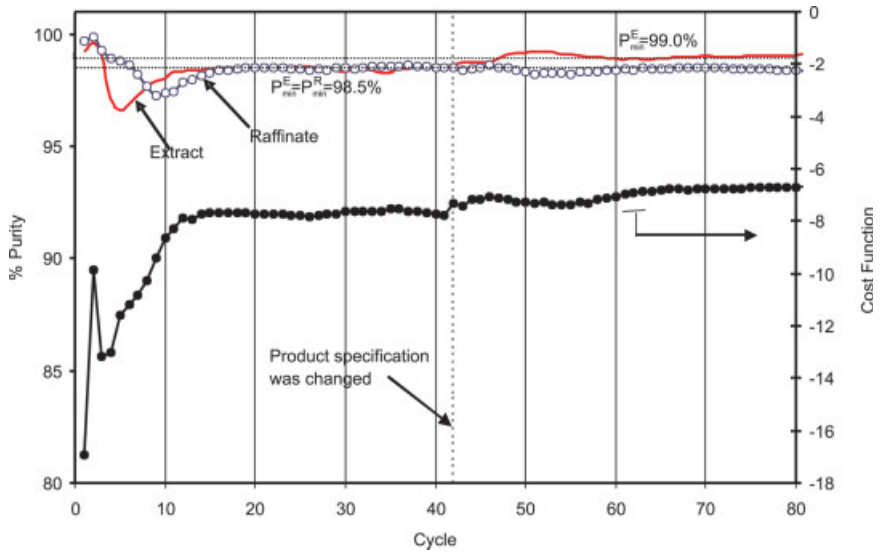

Figure 10. Performance of the controller on the laboratory SMB plant for case study 4.

Outlet purities and cost function vs time measured in cycles. Initially, the specified purity for both outlet streams is 98.5% for the first 42 cycles. At cycle 42 the purity specification for the extract is changed to 99.0%, whereas the purity specification for the raffinate remains 98.5%. [Color figure can be viewed in the online issue, which is available at www.interscience.wiley.com.]

approaches the complete separation region until it reaches its border. Once the minimum purity of the raffinate has been fulfilled, the operation is optimized by moving the operating point towards the vertex of the triangle. In this way, the controller manages to reject this major disturbance, and the operation reaches a steady state that fulfills the requirements for the product specification.

Case study 4: Change in the product purity requirements

Another controlled SMB run is performed to assess the tracking performance of the controller. This scenario addresses a case in which one of the product specifications is changed during the operation. The SMB plant is started up with the same operating parameters as in case study 1, and the controller is switched on cycle 1. The specified purity for both outlets streams is 98.5% at the beginning of the operation. Figure 10 shows the outlet purities and cost function for the entire operation. It can be observed that the specified outlet purities are fulfilled within 20 cycles after the startup. The purity specification of the extract outlet is increased from 98.5% to 99.0% after cycle 42, whereas the purity requirement of the raffinate is kept the same, i.e., 98.5%. One can observe from Figure 10 that the controller fulfills the new extract purity requirement within 18 cycles at the expense of the production cost, and it maintains the purity requirement of the raffinate for the rest of the operation.

The experimental results presented in the case studies 1 to 4 show the capability of the controller to fulfill the purity specifications despite a plant-model mismatch. Furthermore, they show that the disturbances, such as pump malfunctioning, can be rejected efficiently. The results also demonstrate the controller's ability in terms of tracking different purity specifications of the product streams. In summary, the controller assures the product quality and optimizes the performance of the plant, despite major disturbances in the SMB operation.

Assessment of the Performance of the Controller with Time Delay in Measurements Through Simulation

In the previous section, the suitability of the 'cycle to cycle' controller has been demonstrated experimentally for the separation of a mixture of nucleosides that exhibit linear isotherm behavior. We previously underscored that a measurement time delay would occur if HPLC were used for measurement of the outlet streams, especially if the analysis time is longer than the cycle time. In this section, analysis of controller performance under such a scenario for the same system is presented using simulation studies.

Case study 5: Effect of time delay in the measurements

The effect of a time delay in the measurements on the performance of the controller is demonstrated through simulation of a pump malfunctioning scenario. Figure 11 shows the simulation results of the same scenario presented in case study 3, i.e., after reaching a steady operating point that fulfills the specified purities, the recycle pump starts to deliver 5% more than its set point at cycle 56. In this case the measurements have no time delay. The trajectory of the operating point in the $m_{II} - m_{III}$ plane is also shown in this figure. We have discussed these results in detail in case study 3, and it may be worth noting that an excellent agreement is observed between the simulation (Figure 11), and the experimental (Figure 7) runs. The same scenario is simulated again, but adding a time delay of 1 cycle to the measurements. The results are shown in Figure 12. By comparing Figures 11 and

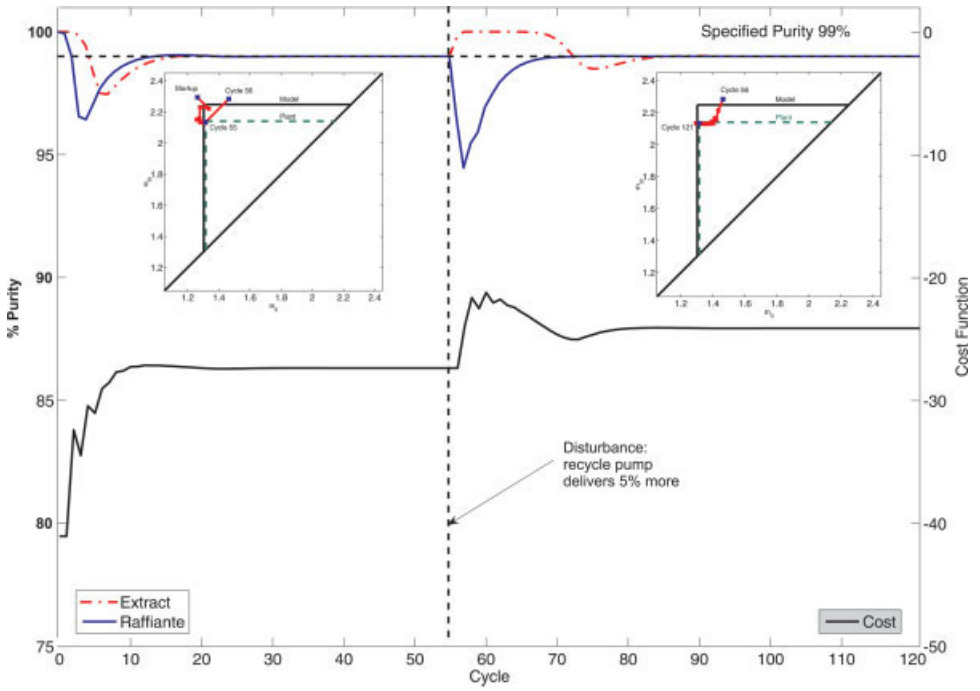

Figure 11. Simulation results with the inherent time delay in the measurements.

Outlet purities and cost function vs time measured in cycles. The right and left boxes present the trajectory of the operation on the $m_{II} - m_{III}$ plane before and after the recycle pump malfunctioning, respectively. [Color figure can be viewed in the online issue, which is available at www.interscience.wiley.com.]

12, a deterioration in the performance can be observed, which is to be expected when the measurements have a time delay. The startup takes 5 cycles more to achieve the specified purities compared to the latter case. After the disturbance, the raffinate and the extract take 5 and 15 cycles more, respectively, to recover. Despite the time delay in the feed-

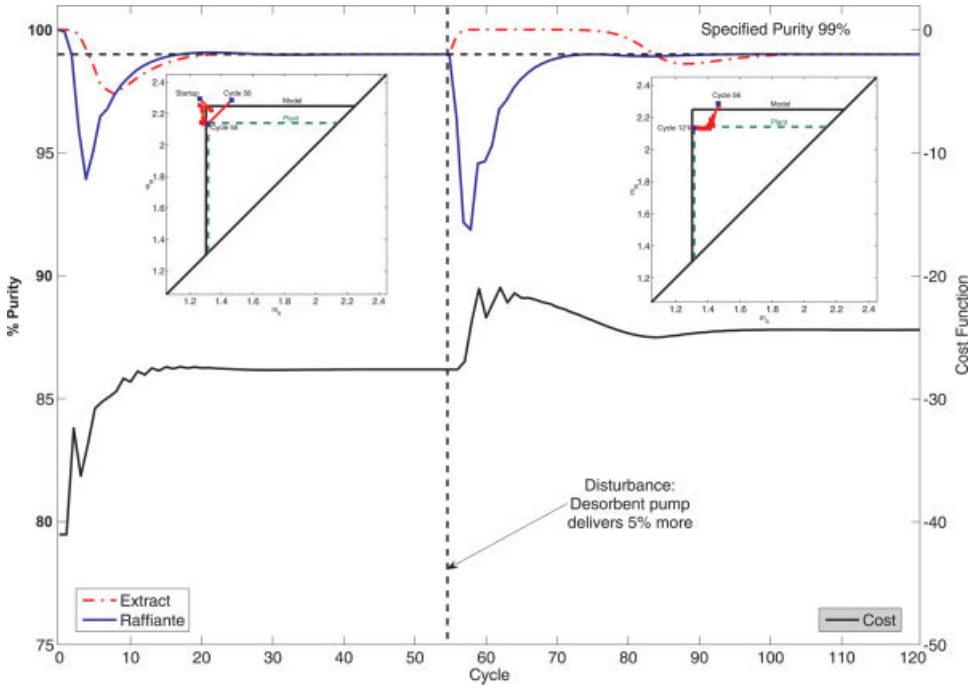

Figure 12. Simulation results with an additional delay of 1 cycle in the measurements.

Outlet purities and cost function vs time measured in cycles. The left and right boxes present the trajectory of the operation on $m_{II} - m_{III}$ plane before and after the recycle pump malfunctioning, respectively. [Color figure can be viewed in the online issue, which is available at www.interscience.wiley.com.]

back information, the qualitative behavior in the $m_{II} - m_{III}$ plane described in the case of no time delay also holds here.

Concluding Remarks

In this study, we have presented the development of the 'cycle to cycle' controller, and its experimental implementation on a laboratory SMB plant for the separation of a mixture of nucleosides. We also assessed the performance of the controller with a time delay in the measurements, through simulations. The experimental runs and simulation studies were designed to challenge the robust performance of the controller. The results have shown that the controller can assure the product quality and optimize the performance of the plant in terms of maximum throughput and minimum desorbent consumption despite uncertainties in the system behavior and major disturbances in the SMB.

The 'cycle to cycle' controller presented and tested in this work is an extension and modification of the online optimization based control concept developed earlier in our group where higher sampling frequencies were used.[18,21,22] Note that the sampling frequency of the experiments presented in the past[18] is 64 times higher than the frequency used for this work. Nevertheless, the performance of the high and low ('cycle to cycle') frequency approaches is comparable despite the drastic reduction in the number of samples taken every cycle.

Furthermore, a thorough comparison has been carried out between the optimal operating point found by the 'cycle to cycle' controller, based on minimal information about the system, and an offline optimization, using a genetic algorithm where all the information about the system was available. For this study, the controller was tested in simulations on four different model systems characterized by generalized Langmuir isotherms, i.e., nonlinear isotherms.[31] The cycle to cycle controller and the offline optimization compare very well. In terms of maximizing the productivity, differences of less than 2% were found between the feed flow rates selected by the controller, and the offline optimization, i.e., the operating points on the $m_{II} - m_{III}$ plane of both approaches lie virtually on top of each other. However, the 'cycle to cycle' controller was less effective in minimizing desorbent consumption, were differences of up to 14 % were found between the desorbent consumption required by the controller and the offline optimization, i.e. the operating points on the $m_I - m_{IV}$ plane are different. This issue will be presented and discussed in more detail in future works.[32]

The usefulness of the 'cycle to cycle' controller primarily emanates from technical limitations in terms of accurate online optical detection and current industrial practice. The novel property of this controller resides in its ability to make use of the concentration of each solute at the outlet streams *averaged over one cycle*, as feedback information. This has special industrial relevance, since systems that collect samples over a given period of time, e.g., a cycle, are already in use as quality control systems. Hence, the industrial implementation of this scheme would be straightforward.

Future works will be aimed at demonstrating that the 'cycle to cycle' control concept is applicable to different operating modes of SMBs, e.g., VARICOL.[24] This approach also sets the basis for the extension of the controller to make use of the full set of operating parameters, i.e., the four internal flow rates and the switch time, to control and optimize the unit.

Acknowledgments

We thank ETH research commission for partially funding this work through project number TH-19/03-3.

Notation

$\underline{A}, \underline{B}, \underline{C}, \underline{D}, \underline{L}, \underline{H}$ = discrete-time state space matrices of the LTV model
$\overline{A}, \overline{B}, \overline{C}, \overline{D}, \overline{L}, \overline{H}$ = state-space matrices of the augmented 'cycle to cycle' SMB model
$\overline{A}^{(n_{td})}, \overline{B}^{(n_{td})}, \overline{C}^{(n_{td})}, \overline{D}^{(n_{td})}, \overline{L}^{(n_{td})}, \overline{H}^{(n_{td})}$ = state-space matrices of the augmented 'cycle to cycle' SMB model in the case of time delay in the measurements
$\mathcal{C}$ = transformation matrix to compute the average concentrations
c = concentration, g/L
$\hat{\mathbf{c}}$ = vector comprising the estimation of the future output concentrations, g/L
ε = bed void fraction
$\mathbf{\Phi}, \mathbf{\Gamma}, \mathbf{\Pi}, \underline{\boldsymbol{G}}$ = state-space matrices of the lifted model
$\mathbf{\Phi}, \mathbf{\Gamma}, \overline{\mathbf{\Pi}}, \overline{\boldsymbol{G}}$ = state-space matrices of 'cycle to cycle' SMB model
$\mathbf{\Phi}, \mathbf{\Gamma}, \mathbf{\Pi}, \boldsymbol{G}$ = state-space matrices of reduced-order 'cycle to cycle' SMB model
$\underline{\boldsymbol{h}}$ = residual term in the model equations
$\overline{\boldsymbol{h}}$ = model prediction error and period-wise persisting disturbances
H_A = Henry constant of component A
H_B = Henry constant of component B
k = cycle index
M = Kalman filter gain matrix
λ = weighting factor in the cost function
m = flow rate ratio
N = number of time steps per cycle
n = time index within a cycle
n_c = control horizon
n_{col} = number of columns constituting the SMB unit
n_{eq} = number of equations in the SMB ODE system
$\tilde{\mathrm{n}}_{eq}$ = number of states of the reduced-order 'cycle to cycle' SMB model
n_g = number of grid points along each column
n_p = prediction horizon
n_{td} = number of cycles of delay in the measurements
n_u = number of inputs
n_y = number of plant outputs
Q = volumetric fluid flow rate, mL/sec
$\boldsymbol{Q}$ = vector comprising the internal flow rates
P = purity of the outlet stream
R_v = covariance matrix of the noise sequence v
R_w = covariance matrix of the noise sequence w
S^z, S^u = prediction matrices
s = slack variable
t^* = switch time, s
u = vector of manipulated variables, mL/sec
$\boldsymbol{U}$ = vector grouping the input values for one cycle
$\mathcal{U}^{n_c}$ = vector of n_c-step future inputs
V = volume of one column, mL
$\boldsymbol{v}, \boldsymbol{w}$ = zero mean white noise sequences
x = state vector
$\tilde{x}$ = state vector of the reduced order model
y = vector of output concentrations, g/L
$\boldsymbol{y}$ = vector of output concentrations, g/L
$\hat{y}$ = estimate of the vector of output concentrations, g/L
$\boldsymbol{Y}$ = vector grouping the output values for one cycle
$\mathcal{Y}^{n_p}$ = vector of n_p-step output predictions
z = state vector of the augmented 'cycle to cycle' SMB model
$\hat{z}$ = estimate of the state vector of the augmented 'cycle to cycle' SMB model

$Z^{(n_{td})}$ = state vector of the augmented 'cycle to cycle' SMB model in the case of time delay in the measurements

Subscripts and superscripts

A = component A-guanosine
ave = average
B = component B-uridine
D = desorbent
E = extract
F = feed
h = column position index, $h = 1, ..,8$
i = component index, $i = A, B$
I, II, III, IV = sections 1, 2, 3, 4 of the SMB plant
j = section index, $j = I..IV$
k = cycle index
max = maximum
min = minimum
$model$ = referring to SMB model
out = column outlet
$plant$ = referring to the SMB plant
R = raffinate
ref = reference values used for linearization

Literature Cited

1. Mazzotti M, Storti G, Morbidelli M. Optimal operation of simulated moving bed units for nonlinear chromatographic separations. *J of Chromatography A*. 1997;769:3–24.
2. Juza M, Mazzotti M, Morbidelli M. Simulated moving-bed chromatography and its application to chirotechnology. *Trends in Biotechnol*. 2000;18:108–118.
3. Kloppenburg E, Gilles ED. Automatic control of the simulated moving bed process for C_8 aromatics separation using asymptotically exact input/output-linearization. *J of Process Control*. 1999;9:41–50.
4. Song I-H, Amanullah M, Erdem G, Mazzotti M, Rhee H-K. Experimental implementation of Identification based optimizing control of a simulated moving bed process. *J of Chromatography A*. 2006;1113:60–73.
5. Song IH, Lee SB, Rhee HK. Identification and predictive control of a simulated moving bed process: Purity control. *Chem Eng Sci*. 2006;61(6):1973–1986.
6. Song IH, Lee SB, Rhee HK, et al. Optimization-based predictive control of a simulated moving bed process using an identified model. *Chem Eng Sci*. 2006;61(18):6165–6179.
7. Schramm H, Grüner S, Kienle A. Optimal operation of simulated moving bed chromatographic processes by means of simple feedback control. *J of Chromatography A*. 2003;1006(1–2):3–13.
8. Klatt KU, Hanisch F, Dünnebier G, Engell S. Model-based optimization and control of chromatographic processes. *Comp and Chem Eng*. 2000;24:1119–1126.
9. Klatt KU, Hanisch F, Dünnebier G. Model-based control of a simulated moving bed chromatographic process for the separation of fructose and glucose. *J of Process Control*. 2002;12:203–219.
10. Wang C, Klatt KU, Dünnebier G, Engell S, Hanisch F. Neural network-based identification of SMB chromatographic processes. *Control Eng Practice*. 2003;11:949–959.
11. Toumi A, Engell S. Optimization-based control of a reactive simulated moving bed process for glucose isomerization. *Chem Eng Sci*. 2004;59:3777–3792.
12. Wang C, Engell S, Hanisch F. Neural network-based identification and MPC control of SMB chromatography. *15th IFAC world congress, Barcelona, Spain*. 2002.
13. Wang C, Klatt KU, Dünnebier G, Engell S, Hanisch F. Neural network-based identification of SMB chromatographic processes. *Control Eng Practice*. 2003;11(8):949–959.
14. Engell S, Toumi A. Optimisation and control of chromatography. *Comp & Chem Eng*. 2005;29(6):1243–1252.
15. Engell S. Feedback control for optimal process operation. *J of Process Control*. 2007;17(3):203–219.
16. Alamir M, Ibrahim F, Corriou JP. A flexible nonlinear model predictive control scheme for quality/performance handling in nonlinear SMB chromatography. *J of Process Control*. 2006;16(4):333–344.
17. Erdem G. *On-line optimization and control of simulated moving bed processes*. ETH Zurich, Switzerland; 2005. PhD thesis.
18. Erdem G, Amanullah M, Morari M, Mazzotti M, Morbidelli M. Optimizing control of an experimental simulated moving bed unit. *AIChE J*. 2006;52(4):1481–1494.
19. Abel S, Erdem G, Mazzotti M, Morari M, Morbidelli M. Optimizing control of simulated moving beds-Linear isotherm. *J of Chromatography A*. 2004;1033(2):229–239.
20. Abel S, Erdem G, Amanullah M, Morari M, Mazzotti M, Morbidelli M. Optimizing control of simulated moving beds – experimental implementation. *J of Chromatography A*. 2005;1092(1):2–16.
21. Erdem G, Abel S, Morari M, Mazzotti M, Morbidelli M, Lee JH. Automatic control of simulated moving beds. *Ind and Eng Chem Res*. 2004;43(2):405–421.
22. Erdem G, Abel S, Morari M, Mazzotti M, Morbidelli M. Automatic control of simulated moving beds-II: Nonlinear isotherm. *Ind and Eng Chem Res*. 2004;43(14):3895–3907.
23. Erdem G, Abel S, Amanullah M, Morari M, Mazzotti M, Morbidelli M. Automatic control of simulated moving beds – Experimental verification. *Adsorption*. 2005;11:573–577.
24. Ludemann-Hombourger O, Nicoud RM, Bailly M. The varicol process: A new multicolumn continuous chromatographic process. *Sep Sci and Technol*. 2000;35:1829–1862.
25. Migliorini C, Gentilini A, Mazzotti M, Morbidelli M. Design of simulated moving bed units under non-ideal conditions. *Ind and Eng Chem Res*. 1999;38:2400–2410.
26. Guiochon G, Golshan-Shirazi S, Katti AM. *Fundamentals of preparative and nonlinear chromatography*. Academic Press; 1994.
27. Kalman RE. A new approach to linear filtering and prediction problems. *Trans ASME, J of Basic Eng*. 1960;82:35–45.
28. Pernebo L, Silverman ML. Model reduction via balanced state space representations. *IEEE Trans on Auto Contr*. 1982;27:382–387.
29. Morari M, Lee JH, Garcia C. *Model Predictive Control, Preprint*. To be published by Prentice-Hall; 2007.
30. MATLAB, *Control System Toolbox*. The MathWorks, Inc.
31. Mazzotti M. Equilibrium theory based design of simulated moving bed processes for a generalized Langmuir isotherm. *J Chromatogr A*. 2006;1126:311–322.
32. Grossmann C, Amanullah M, Morari M, Mazzotti M, Morbidelli M. Optimized control of simulated moving bed separations of mixtures subject to the generalized Langmuir isotherm. *Adsorption*. 2007, in press.

Appendix A. 'Cycle to Cycle' SMB Model with Time Delay in the Output

In this section, general expressions for the matrices $\overline{A}^{(n_{td})}$, $\overline{B}^{(n_{td})}$, $\overline{C}^{(n_{td})}$, $\overline{D}^{(n_{td})}$, $\overline{L}^{(n_{td})}$ and $\overline{H}^{(n_{td})}$ in the 'cycle to cycle' SMB model are derived

$$\begin{aligned} Z_{k+1}^{(n_{td})} &= \bar{A}^{(n_{td})} Z_k^{(n_{td})} + \bar{B}^{(n_{td})} \Delta \mathbf{U}_k + \bar{L}^{(n_{td})} \bar{\bar{\mathbf{w}}}_k \\ \mathbf{y}_k &= \bar{C}^{(n_{td})} Z_k^{(n_{td})} + \bar{D}^{(n_{td})} \Delta \mathbf{U}_k + \bar{H}^{(n_{td})} \bar{\bar{\mathbf{v}}}_k \end{aligned} \tag{A1}$$

In the case of n_{td} cycles of delay, the measured output $\mathbf{y}_k$ at time k is the sum of the average concentrations of cycle $k - 1 - n_{td}$, $\overline{\mathbf{y}}_{k-n_{td}}$ (according to definition Eq. 22), and the effect of random disturbances $\overline{\mathbf{v}}_{k-n_{td}}$, as defined in Eq. 27

$$\mathbf{y}_k \triangleq \overline{\mathbf{y}}_{k-n_{td}} + \overline{\mathbf{v}}_{k-n_{td}} \tag{A2}$$

Furthermore, the augmented state $Z_k^{(n_{td})}$ in the case of a time delay is defined as

$$Z_k^{(n_{td})} = \left[\underbrace{z_k^T}_{\tilde{n}_{eq}+n_y} \quad \underbrace{z_{k-1}^T \quad \cdots \quad z_{k-n_{td}}^T}_{n_{td}\cdot(\tilde{n}_{eq}+n_y)} \quad \underbrace{\Delta \mathbf{U}_{k-1}^T \quad \cdots \quad \Delta \mathbf{U}_{k-n_{td}}^T}_{n_{td}\cdot(N\cdot n_u)} \right]^T \tag{A3}$$

where $z_k^{\mathrm{T}} = [\Delta\tilde{\mathrm{x}}_k(0)^T\ \bar{\mathbf{y}}_k^T]^T$. Note that the first term in Eq. A2, $\bar{\mathbf{y}}_{k-n_{td}}$, is contained within $z_{k-n_{\mathrm{td}}}^T$.

The dimension of the state $Z_k^{(n_{\mathrm{td}})}$ is $n_Z = (n_{td} + 1) \cdot (\tilde{\mathrm{n}}_{eq} + n_y) + n_{td} \cdot (N \cdot n_u)$.

The key idea to arrive to a general expression of the matrices in the Eq. A1, is to describe $\bar{\mathbf{y}}_{k+1}$, contained in the state $Z_{k+1}^{(n_{td})}$, as a function of $\bar{\mathbf{y}}_{k-n_{td}}$, contained in $Z_k^{(n_{\mathrm{td}})}$. For this purpose a register to keep track of the states and inputs between cycle $k - n_{td}$, and k is needed.

The following derivation leads to a general expressions for $\overline{A}^{(n_{td})}$, $\overline{B}^{(n_{td})}$ and $\overline{L}^{(n_{td})}$.

The last row of Eq. 24 is written for $n_{td} + 1$ time steps

$$\begin{array}{lllllll} \bar{\mathbf{y}}_{k+1} & = & \bar{\mathbf{y}}_k & + & \tilde{\mathbf{\Pi}}\Delta\tilde{x}_k(0) & + & \bar{\mathbf{G}}\Delta\mathbf{U}_k & + & \bar{\mathbf{w}}_k \\ \bar{\mathbf{y}}_k & = & \bar{\mathbf{y}}_{k-1} & + & \tilde{\mathbf{\Pi}}\Delta\tilde{x}_{k-1}(0) & + & \bar{\mathbf{G}}\Delta\mathbf{U}_{k-1} & + & \bar{\mathbf{w}}_{k-1} \\ \vdots & & & & & & \vdots & & \\ \bar{\mathbf{y}}_{k-n_{td}+1} & = & \bar{\mathbf{y}}_{k-n_{td}} & + & \tilde{\mathbf{\Pi}}\Delta\tilde{x}_{k-n_{td}}(0) & + & \bar{\mathbf{G}}\Delta\mathbf{U}_{k-n_{td}} & + & \bar{\mathbf{w}}_{k-n_{td}} \end{array} \tag{A4}$$

Successive substitution of the last equation into the previous one, until the first one, gives

$$\bar{\mathbf{y}}_{k+1} = \bar{\mathbf{y}}_{k-n_{td}} + \tilde{\mathbf{\Pi}}\sum_{j=0}^{n_{td}}\Delta\tilde{x}_{k-j}(0) + \bar{\mathbf{G}}\sum_{j=1}^{n_{td}}\Delta\mathbf{U}_{k-j} + \bar{\mathbf{G}}\Delta\mathbf{U}_k + \sum_{j=0}^{n_{td}}\bar{\boldsymbol{w}}_{k-j} \tag{A5}$$

Writing this relationship in matrix form for the augmented state $Z_k^{(n_{td})}$ leads to the desired expressions. Let $\overline{A}^{(n_{td})}$ be a $n_Z \times n_Z$ block matrix of the form

$$\bar{A}^{(n_{td})} = \begin{bmatrix} \mathbf{A}_1^{(n_{td})} \\ \mathbf{A}_2^{(n_{td})} \\ \mathbf{A}_3^{(n_{td})} \\ \mathbf{A}_4^{(n_{td})} \end{bmatrix} \tag{A6}$$

$\overline{\mathbf{A}}_1^{(n_{td})}$ represents the first row of the matrix $\overline{A}$ in Eq. 24 extended for the augmented state, and is given by

$$\mathbf{A}_1^{(n_{td})} = \begin{bmatrix} \tilde{\mathbf{\Phi}} & \underbrace{\mathbf{0}}_{\tilde{n}_{eq}\times(n_Z-\tilde{n}_{eq})} \end{bmatrix} \tag{A7}$$

$\overline{\mathbf{A}}_2^{(n_{td})}$corresponds to the second row of the matrix $\overline{A}$ in Eq. 24 extended for the augmented state, i.e., the first three terms on the RHS of Eq. A5. It is given by

$$\mathbf{A}_2^{(n_{td})} = \begin{bmatrix} \tilde{\mathbf{\Pi}} & \underbrace{\mathbf{J}_1 \quad \cdots \quad \mathbf{J}_1}_{n_y\times n_{td}\cdot(n_y+\tilde{n}_{eq})} & \underbrace{I}_{n_y\times n_y} & \underbrace{\bar{\mathbf{G}} \quad \cdots \quad \bar{\mathbf{G}}}_{n_y\times n_{td}\cdot(N\cdot n_u)} \end{bmatrix} \tag{A8}$$

with $\mathbf{J}_1$

$$\mathbf{J}_1 = \begin{bmatrix} \underbrace{\mathbf{0}}_{n_y\times n_y} & \tilde{\mathbf{\Pi}} \end{bmatrix} \tag{A9}$$

$\overline{\boldsymbol{A}}_3^{(n_{\mathrm{td}})}$ and $\overline{a}_4^{(n_{\mathrm{td}})}$ build a register to keep track of the past states and inputs, respectively. They are given by

$$\mathbf{A}_3^{(n_{td})} = \begin{bmatrix} \underbrace{\mathbf{I}}_{n_{td}\cdot(\tilde{n}_{eq}+n_y)\times n_{td}\cdot(\tilde{n}_{eq}+n_y)} & \underbrace{\mathbf{0}}_{n_{td}\cdot(\tilde{n}_{eq}+n_y)\times(\tilde{n}_{eq}+n_y)+n_{td}\cdot(N\cdot n_u)} \end{bmatrix} \tag{A10}$$

$$\mathbf{A}_4^{(n_{td})} = \begin{bmatrix} \underbrace{\mathbf{0}}_{n_{td}\cdot(N\cdot n_u)\times(\tilde{n}_{td}+1)\cdot(\tilde{n}_{eq}+n_y)} & \mathbf{J}_2^{(n_{td})} & \underbrace{\mathbf{0}}_{n_{td}\cdot(N\cdot n_u)\times(N\cdot n_u)} \end{bmatrix} \tag{A11}$$

with $\mathbf{J}_2^{(n_{\mathrm{td}})}$

$$\mathbf{J}_2^{(n_{td})} = \begin{bmatrix} \mathbf{0} \\ I \end{bmatrix} \tag{A12}$$

where the $\mathbf{0}$ matrix in $\mathbf{J}_2^{(n_{\mathrm{td}})}$ has dimensions of $(N \cdot n_u) \times (n_{td} - 1) \cdot (N \cdot n_u)$, and the identity I matrix has dimensions of $(n_{td} - 1) \cdot (N \cdot n_u) \times (n_{td} - 1) \cdot (N \cdot n_u)$. For the case $n_{td} = 0$, $\mathbf{J}_2^{(n_{\mathrm{td}})}$ is an empty matrix.

The matrix $\overline{B}^{(n_{td})}$ is given by

$$\bar{B}^{(n_{td})} = \begin{bmatrix} \tilde{\mathbf{\Gamma}} \\ \bar{\mathbf{G}} \\ \overline{\mathbf{B}}_1^{(n_{td})} \\ I \\ \overline{\mathbf{B}}_2^{(n_{td})} \end{bmatrix} \tag{A13}$$

The first two rows of $\overline{B}^{(n_{td})}$ correspond to the matrix $\overline{B}$ in Eq. 24. The last three rows serve to store the input $\Delta\mathbf{U}_k^T$ in the state $Z_{k+1}^{(n_{td})} \cdot \mathbf{B}_1^{(n_{\mathrm{td}})}$ and $\mathbf{B}_2^{(n_{\mathrm{td}})}$ are zero matrices with dimensions $n_{td} \cdot (\tilde{n}_{eq} + n_y) \times (N \cdot n_u)$ and $(n_{td} - 1) \cdot (N \cdot n_u) \times N \cdot n_u$, respectively.

The matrix $\overline{L}^{(n_{td})}$ is given by

$$\bar{L}^{(n_{td})} = \begin{bmatrix} \bar{L} \\ \vdots \\ \bar{L} \\ \mathbf{0} \end{bmatrix} \tag{A14}$$

The matrix $\overline{L}$ is contained $(n_{td} + 1)$ times in $\overline{L}^{(n_{td})}$ to add the noise term $\bar{\bar{\boldsymbol{w}}}_k$ to all the terms $\bar{\mathbf{y}}_{k+1} \ldots \bar{\mathbf{y}}_{k-n_{td}}$ contained in $Z_{k+1}^{(n_{td})}$. The zero matrix in the last row of $\overline{L}^{(n_{td})}$ has dimensions $n_{td} \cdot n_y \times n_y$.

The matrix $\overline{C}^{(n_{td})}$ can be expressed as

$$\bar{C}^{(n_{td})} = \begin{bmatrix} \underbrace{0}_{n_y\times(n_{td}+1)\cdot(\tilde{n}_{eq}+n_y)} & \underbrace{I}_{n_y\times n_y} & \underbrace{0}_{n_y\times n_{td}\cdot(N\cdot n_u)} \end{bmatrix} \tag{A15}$$

$\overline{D}^{(n_{td})}$ is a zero matrix with dimensions of $n_y \times (N \cdot n_u)$. $\overline{H}^{(n_{td})}$ is an identity matrix with dimensions $n_y \times n_y$.

Manuscript received Apr. 19, 2007, and revision received Aug. 17, 2007.